Nonlinear vibration of a single-walled carbon nanotube embedded in a polymer matrix aroused by interfacial van der Waals forces

M. H. Mahdavi, L. Y. Jiang,[a)] and X. Sun
Department of Mechanical and Materials Engineering, The University of Western Ontario, London, Ontario N6A 5B9, Canada

This paper studies the nonlinear vibration of a single-walled carbon nanotube (CNT) embedded in a polymer matrix aroused by van der Waals (vdW) forces using elastic beam models. The interfacial vdW forces are described by a nonlinear function in terms of the deflection of the CNT. According to different beam end conditions, the relation between deflection amplitudes and resonant frequencies of free vibrations of the CNT is derived through harmonic balance method. This relation is found to be sensitive to end conditions, diameters, and lengths of the embedded CNT. The axial load effect upon the vibrational behavior of the CNT and postbuckling of the embedded CNT are also discussed. Due to the influence of the surrounding polymer, the prediction on the critical buckling loads and resonant frequencies for embedded CNTs is quite different from that for free-standing CNTs. In addition, the applicability and accuracy of both Euler–Bernoulli and Timoshenko beam models are investigated. It is found that the Euler–Bernoulli beam model may provide comparable results as the Timoshenko beam model even for CNTs with smaller length-to-diameter ratios due to the constraint from the surrounding medium. © *2009 American Institute of Physics*. [doi:10.1063/1.3266174]

I. INTRODUCTION

In recent years, researchers have advanced the field of nanotechnology at a phenomenal pace since the discovery of carbon nanotubes (CNTs) by Iijima.[1] Extensive studies on these novel materials have showed that CNTs possess exceptional mechanical, electronic, and thermal properties.[2–7] These extraordinary physical properties make CNTs promising candidates for many potential applications as nanoelectronics, nanodevices, and nanocomposites.[8–15]

Mechanical behavior of CNTs, including vibrational behavior, has become a popular topic in numerous studies. Due to extreme difficulties in conducting experiments on nanoscale materials and computing expensiveness of atomic studies, many researchers have pursued the analysis of CNTs by continuum mechanics models. For example, there are many available papers in which elastic beam models[16–23] and elastic shell models[24–28] have been effectively used to predict resonant frequencies and buckling behavior of CNTs. Through these studies and many others, it has been indicated that "the laws of continuum mechanics are amazing robust and allow one to treat even intrinsically discrete objects only a few atoms in diameter."[29]

It should be mentioned that most existing continuum studies of CNTs are linear analyses. Until recently, there are several investigations on the matter of different aspects of nonlinearities in CNTs. Fu *et al.*[19] studied the nonlinear free vibration of an embedded multiwalled CNT (MWCNT) considering the geometric nonlinearity of the beam model. The surrounding matrix interaction force and the van der Waals (vdW) interaction between two adjacent tubes were assumed

to be linear. It was shown in this work that the nonlinear free vibration of CNTs is affected significantly by the surrounding elastic medium. The nonlinear vibration of a double-walled carbon nanotube (DWCNT) aroused by the nonlinear interlayer vdW forces was studied by Xu *et al.*[18] The deflection amplitude was revealed to decreases in square with the increase in the nonlinear coefficient of the interlayer vdW force. It was also shown that the nonlinear factor of the vdW force has little effect on the coaxial free vibration but a great effect on the noncoaxial free vibration. Considering the nonlinearity due to large transverse displacements, Yan *et al.*[27] predicted the nonlinear vibration behavior of a DWCNT based on Donnell's cylindrical shell model with linear vdW force between the inner and outer tubes. The nonlinear postbuckling behavior of CNTs under large strain has also attracted great attention from some researchers.[28,30,31]

Due to the fact that CNTs are often embedded in a polymer or a metal matrix in many applications, considerable attention has turned to the mechanical behavior of the embedded single or MWCNTs. The enhancement in stiffness and strength due to the addition of CNTs in polymeric materials has been established.[13,15,32–34] Because electronic and transport properties of CNTs could be extremely sensitive to their vibration modes and resonant frequencies, the investigation on the dynamic characteristics and instabilities of CNTs is very significant for the application and design of various nanodevices and nanocomposites, in which CNTs act as basic elements. Hence, the study of the vibration, frequency analysis, and buckling of embedded CNTs is a major topic of current interest.[19–26,34–38]

In the existing studies, the effect of the surrounding medium upon embedded CNTs was commonly described by a Winkler-like model, which was originally developed for a

---

a)Author to whom correspondence should be addressed. Electronic mail: lyjiang@eng.uwo.ca.

fiber composite.[39] By using this model, the medium is assumed to act as linear springs and the pressure at any point between the outer tube and the elastic matrix is linearly proportional to the deflection of the outermost tube at that point.[20–26,35] However, the nanoscale interaction between the CNT and the surrounding medium at interface is governed by the vdW force in the absence of covalent chemical bonds and mechanical interlocking. This vdW force is intrinsically nonlinear and its nonlinearity might play an important role in the vibrational and postbuckling behaviors of the embedded CNT, especially when the relation between deflection amplitudes and the resonant frequencies of CNTs is considered. To the authors' knowledge, such an atomistic-based nonlinear interaction effect has not been studied in the existing continuum modeling. Therefore, the objective of the current work is to investigate the nonlinear vibration of an embedded CNT aroused by the nonlinear vdW interaction forces from the surrounding medium using elastic beam models. The effects of axial load and different CNT end conditions on the nonlinear vibration of the embedded CNT are also examined. Moreover, the critical buckling load and postbuckling behavior are predicted to show the surrounding medium effect. The obtained results indicate that the surrounding medium has a substantial effect upon the vibrational and the stability behavior of the embedded CNT.

II. ANALYTICAL MODELS AND SOLUTIONS

Since the classical Euler–Bernoulli beam model can give a simple and reliable prediction on the mechanical behavior of CNTs under some circumstances, the resonant frequencies and postbuckling behavior of the embedded CNT will be studied by this continuum model. To capture the effects of rotary inertia and the shear deformation, which are essential for frequency analysis either at ultrahigh frequencies or for CNTs with low length-to-diameter aspect ratio,[22] a Timoshenko beam model is also adopted for comparison. First, we formulate the nonlinear expression of the resultant pressure exerted by the surrounding polymer matrix to the CNT from an interfacial cohesive law[40] based on the vdW forces only.

A. Nonlinear expression of the vdW interaction forces

In the absence of covalent bonds and mechanical interlocking between CNT and polymer matrix, the interaction between the CNT and its surrounding medium comes from vdW forces, which can be described by Lennard-Jones potential. Notice that the radius effect of CNT upon the interaction potential energy is not significant;[40] this interaction between CNT and polymer matrix can be well estimated by the cohesive energy per unit area between a graphene and a polymer matrix. Based on the Lennard-Jones potential, Jiang *et al.*[40] derived a cohesive law for the interface with cohesive energy being expressed in terms of the interfacial spacing δ as

$$\Phi(\delta) = \frac{2\pi}{3}\rho_P\rho_C\varepsilon\delta_0^3\left(\frac{2\delta_0^9}{15\delta^9} - \frac{\delta_0^3}{\delta^3}\right), \tag{1}$$

where ε is the energy at the equilibrium distance and $\sqrt[6]{2}\delta_0$ is the equilibrium distance between the interacting atoms, and the values of these two parameters vary with the interacting atoms. If the polymer matrix is polyethylene, for example, they take the values $\varepsilon=0.004\,656$ eV and $\delta_0=0.3825$ nm for the interacting carbon atoms of the CNT and the $-CH_2-$ repeating units of the polyethylene. $\rho_C=3.8177 \times 10^{19}$ at./m^2 and $\rho_P=0.3052$ at./m^3 are the area density of carbon atoms on the graphene and the volume density of polymer molecules, respectively. One can easily find the equilibrium interfacial spacing δ_e from Eq. (1) as $\delta_e=(2/5)^{1/6}\delta_0$, and the interaction force per unit area exerted on the CNT surface is derived as[40]

$$P(\delta) = \frac{\partial\Phi}{\partial\delta} = 2\pi\rho_P\rho_C\varepsilon\delta_0^2\left(\frac{\delta_0^4}{\delta^4} - \frac{2}{5}\frac{\delta_0^{10}}{\delta^{10}}\right). \tag{2}$$

As argued by Ru[24] for the interaction pressure between different layers of CNTs, the resultant interaction pressure exerted on the CNT defined per unit length should be proportional to the circumferential dimension, for example, the radius R of CNT. Thus one can assume that the resultant interaction pressure per unit axial length between CNT and the surrounding polymer matrix is $p=-2RP(\delta)$. Notice that this resultant pressure is an odd function about the interfacial equilibrium spacing δ_e. Similar to the nonlinear pressure between adjacent tubes derived for the DWCNT,[18] the Taylor expansion of p at δ_e can be expanded up to the lowest-order nonlinear term as

$$p = -2RP|_{\delta=\delta_e} - 2R\left.\frac{\partial P}{\partial\delta}\right|_{\delta=\delta_e}(\delta-\delta_e)$$
$$-2R\frac{1}{6}\left.\frac{\partial^3 P}{\partial\delta^3}\right|_{\delta=\delta_e}(\delta-\delta_e)^3 = -\alpha_1 w - \alpha_3 w^3, \tag{3}$$

where

$$\alpha_1 = 2R\left.\frac{\partial P}{\partial\delta}\right|_{\delta=\delta_e} = 16\pi\rho_P\rho_C\varepsilon\delta_0 R\left(\frac{\delta_0^{11}}{\delta_e^{11}} - \frac{\delta_0^5}{\delta_e^5}\right), \alpha_3$$
$$= 2R\frac{1}{6}\left.\frac{\partial^3 P}{\partial\delta^3}\right|_{\delta=\delta_e} = 16\pi\rho_P\rho_C\varepsilon\frac{1}{\delta_0}R\left(22\frac{\delta_0^{13}}{\delta_e^{13}} - \frac{\delta_0^7}{\delta_e^7}\right), \tag{4}$$

are the equivalent linear and nonlinear stiffness of the surrounding medium and the first term $P|_{\delta=\delta_e}=0$ in Eq. (3). The interfacial spacing change equals to the deflection w of CNT, i.e., $\delta-\delta_e=w$.

B. Euler–Bernoulli beam model

In the Euler–Bernoulli beam model, the deflection $w(x,t)$ of an elastic beam under distributed lateral pressure p and constant compressive axial force F is governed by

$$EI\frac{\partial^4 w}{\partial x^4} + F\frac{\partial^2 w}{\partial x^2} + \rho A\frac{\partial^2 w}{\partial t^2} = p, \tag{5}$$

where the lateral pressure p comes from the surrounding medium as given in Eq. (3). E and ρ are Young's modulus and the mass density of the CNT, and I and A are the second moments of area and cross-sectional area, defined for a hollow cylinder as

$$I = \frac{\pi}{64}[(d+t)^4 - (d-t)^4], \quad A = \frac{\pi}{4}[(d+t)^2 - (d-t)^2], \tag{6}$$

with $t = 0.35$ nm (Refs. 20–22) being the wall thickness of the single-walled CNT. By assuming $w(x,t) = W\sin(\omega t)Y_1(x)$ with W and $Y_1(x)$ representing the deflection amplitude of the CNT and the first vibrational mode of the system, respectively, Eq. (5) can be rewritten as

$$EI\frac{d^4 Y_1(x)}{dx^4} + F\frac{d^2 Y_1(x)}{dx^2} - \rho A\omega^2 Y_1(x) = -\alpha_1 Y_1(x)$$
$$- \alpha_3[Y_1(x)]^3 W^2 \sin^2 \omega t. \tag{7}$$

Equation (7) reduces to the governing equation of a linear system simply by letting $\alpha_3 = 0$. Assuming $Y_1(x) = \exp(\lambda_1 x)$ in which λ_1 is the first eigenvalue of the linear equation, the first resonant frequency for the linear system can be obtained provided the end conditions for CNT are given. It should be noted that the linear vibration analysis cannot determine the deflection amplitudes of the free vibrational modes. However, the deflection amplitude is frequency dependent and can be determined by a nonlinear vibration analysis. By using harmonic balance method,[18,41] Eq. (7) becomes

$$E_1 + FE_2 - E_3\omega^2 + E_4 + E_5 W^2 = 0, \tag{8}$$

in which

$$E_1 = EI\lambda_1^4 \int_0^L [Y_1(x)]^2 dx \int_0^{2\pi/\omega} \sin^2 \omega t\, dt, \tag{9a}$$

$$E_2 = \lambda_1^2 \int_0^L [Y_1(x)]^2 dx \int_0^{2\pi/\omega} \sin^2 \omega t\, dt, \tag{9b}$$

$$E_3 = \rho A \int_0^L [Y_1(x)]^2 dx \times \int_0^{2\pi/\omega} \sin^2 \omega t\, dt, \tag{9c}$$

$$E_4 = \alpha_1 \int_0^L [Y_1(x)]^2 dx \times \int_0^{2\pi/\omega} \sin^2 \omega t\, dt, \tag{9d}$$

$$E_5 = \alpha_3 \int_0^L [Y_1(x)]^4 dx \times \int_0^{2\pi/\omega} \sin^4 \omega t\, dt. \tag{9e}$$

Through Eqs. (8) and (9), for the case of a linear vibration of CNT considering the effects of both the linear vdW force ($\alpha_3 = 0$) and the axial force F, the first linear resonant frequency $\omega_{1,LE}$ predicted by the Euler–Bernoulli beam model is derived as

$$\omega_{1,LE}^2 = \frac{EI\lambda_1^4 + F\lambda_1^2 + \alpha_1}{\rho A}. \tag{10}$$

Particularly, if the axial load effect is ignored with $F = 0$, Eq. (10) can be simplified as

$$\omega^2 = \left(\frac{EI\lambda_1^4 + \alpha_1}{\rho A}\right)^{1/2}, \tag{11}$$

which gives the same formula developed by Amin et al.[22] for the resonant frequency of an embedded CNT. After simplification, the relation between the deflection amplitude and the first nonlinear resonant frequency of a CNT embedded in a polymer medium aroused by the nonlinear vdW forces is given by the Euler–Bernoulli beam model in the following form:

$$\omega_{1,NE}^2 = \omega_{1,LE}^2 + \frac{3\alpha_3 W^2}{4\rho A}\frac{\int_0^L [Y_1(x)]^4 dx}{\int_0^L [Y_1(x)]^2 dx}. \tag{12}$$

C. Timoshenko beam model

Once the shear deformation and the rotary inertia effects are considered, the vibration of Timoshenko beam under a constant axial force F and a nonlinear lateral pressure p is described by coupled differential equations:

$$KAG\left(\frac{\partial^2 w}{\partial x^2} - \frac{\partial \psi}{\partial x}\right) - F\frac{\partial \psi}{\partial x} + p = \rho A\frac{\partial^2 w}{\partial t^2}, \tag{13a}$$

$$EI\frac{\partial^2 \psi}{\partial x^2} + (F + KAG)\left(\frac{\partial w}{\partial x} - \psi\right) = \rho I\frac{\partial^2 \psi}{\partial t^2}, \tag{13b}$$

where w and ψ are the lateral deflection and angular deflection of the cross section of the beam with respect to the vertical direction. $G = E/2(1+v)$ is shear modulus with v being the Poisson's ratio. Since the present CNT is treated as a single beam with hollow annular cross section, the dependence of the shear correction factor K on its cross-sectional shape is determined as $K = 2(1+v)/(4+3v)$.[42]

The harmonic solutions of a Timoshenko beam can be expressed as

$$w(x,t) = W\sin(\omega t)Y_1(x), \tag{14a}$$

$$\psi(x,t) = \Psi\sin(\omega t)\Phi_1(x). \tag{14b}$$

Substituting Eqs. (14a) and (14b) into Eqs. (13a) and (13b) results in

$$KAG\left(\frac{d^2 Y_1(x)}{dx^2} - \frac{d\Phi_1(x)}{dx}\right) - F\frac{d\Phi_1(x)}{\partial x} - \alpha_1 Y_1(x)$$
$$- \alpha_3[Y_1(x)]^3 W^2 \sin^2 \omega t = -\rho A\omega^2 Y_1(x), \tag{15a}$$

$$EI\frac{d^2 \psi}{dx^2} + (F + KAG)\left(\frac{dY_1(x)}{dx} - \Phi_1(x)\right) = -\rho I\omega^2 \Phi_1(x). \tag{15b}$$

After manipulating Eqs. (15a) and (15b), the following decoupled governing equations can be obtained for the Timoshenko beam,

$$\frac{d^4Y_1(x)}{dx^4} + H_1\frac{d^2Y_1(x)}{dx^2} + H_2Y_1(x) + \alpha_3W^2\sin^2\omega tH_3 = 0,$$

$$(16a)$$

$$\frac{d^4\Phi_1(x)}{dx^4} + H_1\frac{d^2\Phi_1(x)}{dx^2} + H_2\Phi_1(x) + \alpha_3W^2\sin^2\omega tH_3 = 0,$$

$$(16b)$$

where

$$H_1 = \frac{\rho A\omega^2 - \alpha_1}{KAG} + \frac{\rho\omega^2}{E} + \frac{F}{EI} + \frac{F^2}{EIKAG},$$

$$(17a)$$

$$H_2 = \frac{\rho A\omega^2 - \alpha_1}{EIKAG}(\rho I\omega^2 - F - KAG),$$

$$(17b)$$

$$H_3 = -\frac{3}{KAG}\left\{[Y_1(x)]^2\frac{d^2Y_1(x)}{dx^2} + 2Y_1(x)\left[\frac{dY_1(x)}{dx}\right]^2\right\}$$

$$-\frac{\rho I\omega^2 - F - KAG}{EIKAG}[Y_1(x)]^3.$$

$$(17c)$$

Following the same procedure for the Euler–Bernoulli beam model, the relationship between the lateral deflection amplitude W and the first nonlinear resonant frequency $\omega_{1,NT}$ of the embedded CNT predicted by the Timoshenko beam model is derived after lengthy calculations,

$$\omega_{1,NT}^4 + N_1\omega_{1,NT}^2 + N_2 = 0,$$

$$(18)$$

where

$$N_1 = \frac{E + KG}{\rho}\lambda_1^2 - \frac{F + KAG}{\rho I} - \frac{\alpha_1}{\rho A} - \frac{3\alpha_3W^2}{4\rho A}\frac{\int_0^L[Y_1(x)]^4dx}{\int_0^L[Y_1(x)]^2dx},$$

$$(19a)$$

$$N_2 = \frac{\lambda_1^2 EI(\lambda_1^2KAG - \alpha_1) + (F + KAG)(F\lambda_1^2 + \alpha_1)}{\rho^2 AI}$$

$$+ \frac{3\alpha_3W^2}{4\rho^2 AI}\frac{\int_0^L[Y_1(x)]^4dx}{\int_0^L[Y_1(x)]^2dx}(F + KAG - 9\lambda_1^2EI).$$

$$(19b)$$

It should be noted that the linear resonant frequency of the embedded CNT calculated by the Timoshenko beam theory can be similarly obtained by letting $\alpha_3 = 0$ in Eqs. (18) and (19).

D. Evaluation of the buckling load

In the analysis of postbuckling behavior of structures, one of the most interesting problems is to find out the relation between the applied loads and the deflection amplitudes, the so-called postbuckling equilibrium path.[43] Considering a compressive force acting on a column which increases from zero up to its critical value, as the amount of force increases, the equivalent stiffness of the column will decrease and becomes zero when the force becomes enough close to its critical value.[44] When the compressive axial force equals to the first critical buckling load, the first natural frequency of the beam becomes zero. Therefore, the relation between the axial buckling load and the lateral deflection amplitude of the em-

bedded CNT can be obtained by substituting $\omega = 0$ into Eqs. (12) and (18) for an Euler–Bernoulli beam and a Timoshenko beam, respectively. For example, considering the nonlinear vdW force, the relation between the first postbuckling load F_{NE} and the CNT deflection amplitude W predicted by the Euler–Bernoulli beam theory is derived as

$$F_{NE} = F_{LE}^{cr} - \frac{3\alpha_3W^2}{4\lambda_1^2}\frac{\int_0^L[Y_1(x)]^4dx}{\int_0^L[Y_1(x)]^2dx},$$

$$(20)$$

where $F_{LE}^{cr} = -(EI\lambda_1^4 + \alpha_1)/\lambda_1^2$ is the first critical buckling load predicted for an Euler–Bernoulli beam without considering the nonlinear effect of the vdW force, which is independent of the deflection amplitude. By letting $\omega = 0$ in Eq. (18), the corresponding relation between the first postbuckling load of an embedded CNT in a matrix and the deflection amplitude predicted by the Timoshenko beam theory can be similarly obtained from the following equation:

$$F_{NT}^2 + M_1F_{NT} + M_2 = 0,$$

$$(21)$$

where

$$M_1 = KAG + \frac{\alpha_1}{\lambda_1^2} + \frac{3\alpha_3W^2}{4\lambda_1^2}\frac{\int_0^L[Y_1(x)]^4dx}{\int_0^L[Y_1(x)]^2dx},$$

$$(22a)$$

$$M_2 = EI(\lambda_1^2KAG - \alpha_1) + \frac{KAG\alpha_1}{\lambda_1^2}$$

$$+ \frac{3\alpha_3W^2}{4\lambda_1^2}\frac{\int_0^L[Y_1(x)]^4dx}{\int_0^L[Y_1(x)]^2dx}(KAG - 9\lambda_1^2EI).$$

$$(22b)$$

III. NUMERICAL RESULTS AND DISCUSSIONS

According to different end conditions [simply supported support (S-S) and clamped-clamped (C-C)] and length-to-diameter aspect ratios, the relationship between the deflection amplitudes and the resonant frequencies and the postbuckling behavior of the embedded CNT will be studied using both Euler–Bernoulli and Timoshenko beam models. In numerical simulation, it is assumed that Young's modulus, Poisson's ratio, and mass density for the embedded CNT are $E = 1$ TPa, $v = 0.34$, and $\rho = 1.3$ g/cm^3, respectively,[20–22] and the surrounding medium of CNT is polyethylene.

Based on the Euler–Bernoulli beam model, the first vibrational modes are derived as

$$Y_1(x) = \sin\lambda_1x, \quad \lambda_1 = \frac{\pi}{L}$$

$$(23)$$

and

$$Y_1(x) = \sinh\lambda_1x - \sin\lambda_1x$$

$$+ \frac{\sinh\lambda_1L - \sin\lambda_1L}{\cos\lambda_1L - \cosh\lambda_1L}(\cosh\lambda_1x - \cos\lambda_1x),$$

$$\lambda_1 = \frac{4.730}{L}$$

$$(24)$$

for the beam with S-S end condition and C-C end condition, respectively.[45] Substituting λ_1 in Eqs. (23) and (24) into Eq. (12) results in the corresponding resonant frequencies for the
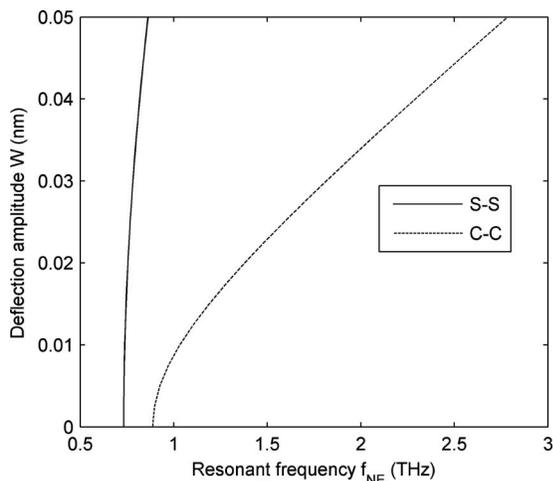
FIG. 1. Vibrational mode of an embedded CNT with different end conditions ($d=0.7$ nm and $L=10d$).

Euler–Bernoulli beam with different end conditions. Unlike the linear vibration, these resonant frequencies relate to the deflection amplitudes. Without considering the axial load effect, Fig. 1 shows the vibration amplitude versus the resonant frequency $f=\omega/2\pi$ for an embedded CNT with diameter d $=0.7$ nm and length $L=10d$ using an Euler–Bernoulli beam model. When the deflection amplitude is zero, the corresponding resonant frequencies aroused by the linear part of the vdW force are determined as 0.7329 THz for the S-S end condition and 0.8875 THz for the C-C end condition, respectively. For the case of the S-S end condition, when the deflection amplitude increases from 0 up to 0.05 nm, the resonant frequency increases from 0.7329 to 0.8628 THz. This jump is more pronounced for the beam with the C-C end condition, for example, the resonant frequency increases from 0.8875 to 2.7847 THz with the deflection amplitude increasing from 0 to 0.05 nm. According to the curves in Fig. 1, the amplitude increases by approximately 5.5×10^{-8} nm for the S-S end condition and 1.0×10^{-8} nm for the C-C end condition along with the resonant frequency increasing by 1 Hz from the linear resonant frequency. It is obvious that the CNT deflection amplitude has a higher sensitivity to the resonant frequency change for the S-S end condition in comparison with the C-C end condition.

In order to reveal the CNT size effect on the nonlinear resonant frequencies and the deflection amplitudes of the embedded CNT, the deflection amplitude-frequency curves of CNTs with different diameters for both S-S and C-C end conditions of an Euler–Bernoulli beam are depicted in Fig. 2 for comparison. The length-to-diameter ratio is kept constant as $L/d=20$. It is indicated in this figure that the resonant frequencies of the embedded CNT decrease with the increase in the CNT diameter for both S-S and C-C end conditions. However, when the CNT size is relatively big, for example, $d>2.1$ nm, the CNT size effect upon the resonant frequencies is not significant. Moreover, the deflection amplitude for a nonlinear vibrational CNT with a larger diameter is higher for any given resonant frequency. It is also found in this figure that the amplitudes for the CNT with the S-S end condition are raised more rapidly along with the increasing
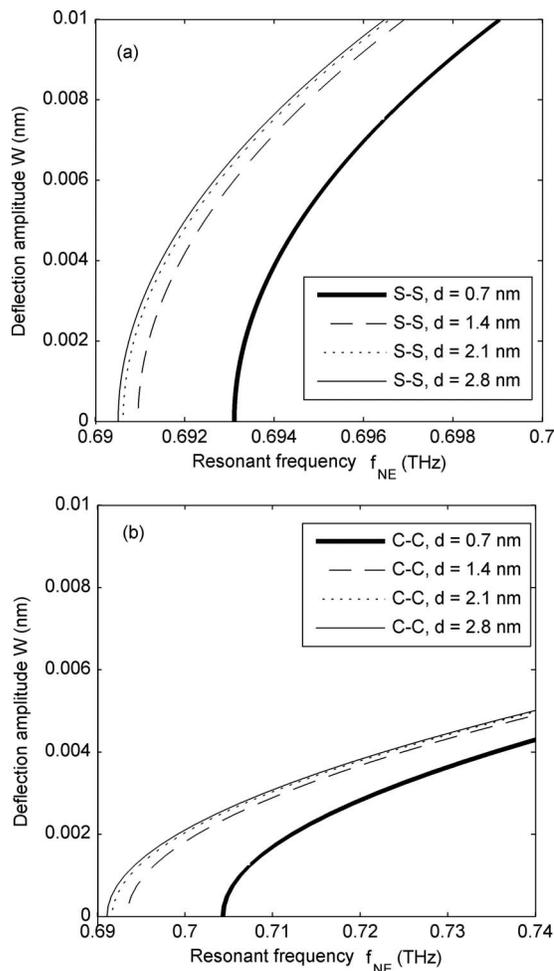
FIG. 2. CNT size effect on the resonant frequencies of an embedded CNT with (a) S-S and (b) C-C end conditions ($L=20d$).

resonant frequencies. Based on the Euler–Bernoulli beam theory, Fig. 3 shows the effect of the CNT length on the nonlinear resonant frequencies of an embedded CNT with fixed diameter $d=0.7$ nm for both S-S and C-C end conditions. It is found that the resonant frequencies decrease with the increase in the length-to-diameter ratio. In addition, for a given resonant frequency, the deflection amplitude for a nonlinear vibrational CNT with a higher length-to-diameter ratio is larger. However, when the length-to-diameter ratio is big enough, for example, $L/d>30$ in the current case, the resonant frequencies do not change much. Similar to Fig. 2, the end condition has a significant effect on the resonant frequencies.

Since the Euler–Bernoulli beam model may not provide accurate prediction for the vibrational behavior of a CNT when the length-to-diameter ratio is less than 20, the Timoshenko beam model is also adopted to complement this study. The first vibrational mode of the Timoshenko beam with the S-S end condition is the same as that of the Euler–Bernoulli beam model in Eq. (23). Similarly, the deflection amplitude-frequency relation can be determined through Eqs. (18), (19), and (23). Figure 4 shows the nonlinear resonant frequencies of an embedded CNT with $d=0.7$ nm and L $=10d$, obtained by both Euler–Bernoulli and Timoshenko beam models with the S-S end condition. It is found that the
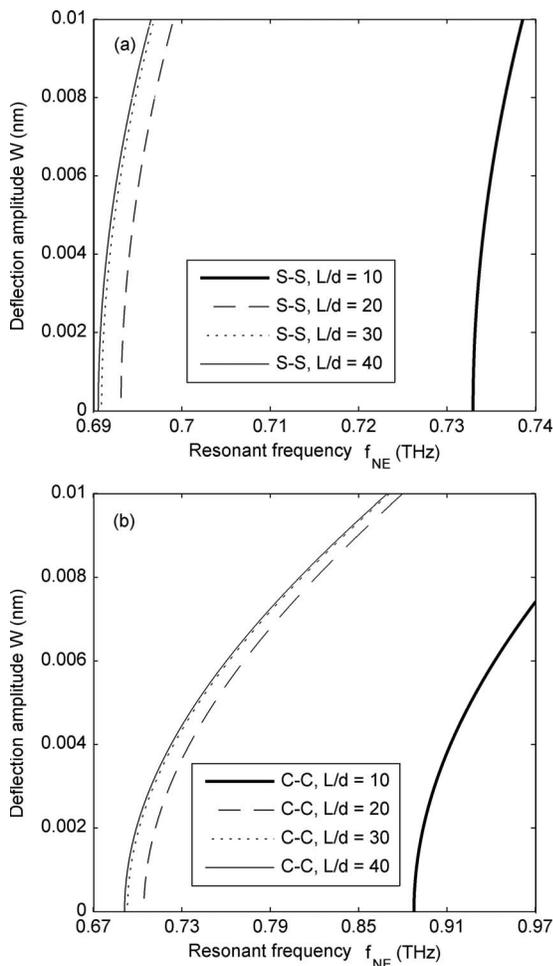
FIG. 3. Effect of CNT length-to-diameter ratio on the resonant frequencies of an embedded CNT with (a) S-S and (b) C-C end conditions (d =0.7 nm).

Timoshenko beam theory is capable of capturing two different frequencies as discussed by Rao.[45] The smaller value given by the Timoshenko theory corresponds to the bending deformation mode which is very close to the resonant frequency given by the Euler–Bernoulli beam model, while the larger one corresponds to the shear deformation mode. The second Timoshenko resonant frequency does not change much with the deflection amplitude. The Euler–Bernoulli beam theory does not account for the effects of the shear deformation and the rotary inertia. As a result, it underestimates the deflections and overestimates the natural frequencies for a linear vibration. The inset of Fig. 4 confirms this claim when the deflection amplitude is zero, which is equivalent to a linear vibration with predicted resonant frequencies being 0.7251 and 0.7320 THz for the Timoshenko beam model and the Euler Bernoulli beam model, respectively. For a nonlinear vibration, as long as the deflection amplitude is smaller than a specific value, 0.0156 nm, for example, in the current case, the Euler–Bernoulli beam model overestimates the resonant frequencies for the bending deformation mode. However, when the deflection amplitude is higher than the above-mentioned value, the Euler–Bernoulli beam model underestimates the resonant frequencies. A similar phenomenon was observed by Ramezani et al.[46] when the shear deforma-
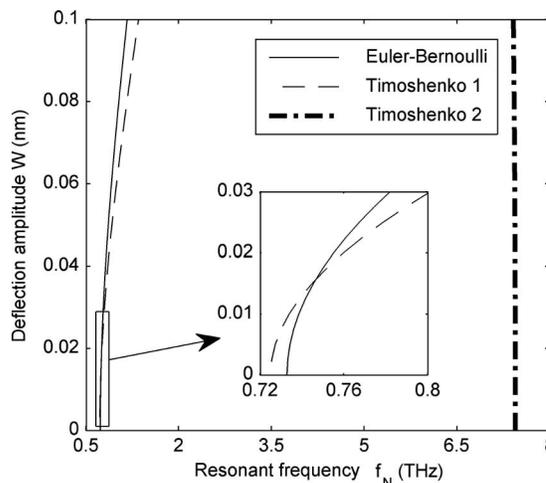
FIG. 4. Vibrational mode of an embedded CNT for different beam models with S-S end condition (d=0.7 nm and L=10d).

tion and rotary inertia effects are considered for the nonlinear vibration analysis of a microbeam without the constraint of the surrounding medium. It should be noted that for both Euler–Bernoulli and Timoshenko beam models, the resonant frequencies increase with the increase in the deflection amplitudes.

The axial load effect on the vibrational behavior of the embedded CNT with diameter d=0.7 nm and length L =20d is plotted in Fig. 5 predicted by the Euler–Bernoulli beam model for different end conditions. The axial load is applied as a compressive strain ε. As expected, the resonant frequency decreases with the axial compressive strain since this applied load softens the beam. Particularly, the linear resonant frequencies corresponding to ε=0, 0.05, and 0.1 are 0.6931, 0.6568, and 0.6183 THz for the S-S end condition and 0.7043, 0.6204, and 0.5231 THz for the C-C end condition, respectively. When this applied axial load equals to the first critical buckling load, the resonant frequency decreases to zero as discussed in Sec. II. Since the curves for the C-C end condition approach the origin faster with the increasing applied strain, it is expected that the critical buckling strain
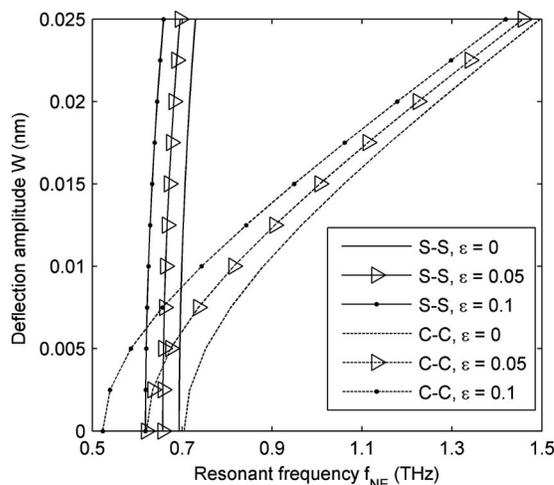
FIG. 5. Effect of the axial load on the resonant frequencies of an embedded CNT (d=0.7 nm and L=20).
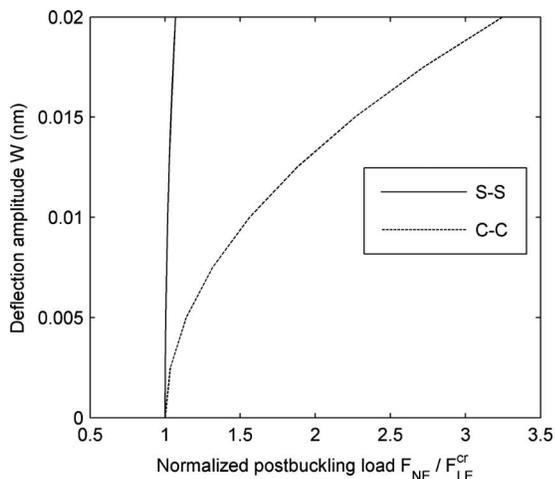
FIG. 6. Postbuckling behavior of an embedded CNT with different end conditions ($d=0.7$ nm and $L=20d$).

FIG. 7. Postbuckling behavior of an embedded CNT using different beam models with S-S end condition ($d=0.7$ nm and $L=10d$).

for the embedded CNT with the C-C end condition is smaller than that of a CNT with the S-S end condition, which is contrary to the fact of the critical buckling strain of a pure compressive column. Such a discrepancy is believed to attribute to the surrounding medium effect, i.e., the second term in the first critical buckling load $F_{LE}^{cr}=-(EI\lambda_1^4+\alpha_1)/\lambda_1^2$ is dominant.

The effect of the nonlinear vdW force from the surrounding medium upon the postbuckling behavior of the embedded CNT is also examined. Figure 6 shows the postbuckling equilibrium paths for the embedded CNT with different end conditions. In this figure, the postbuckling load is normalized by the first critical buckling load F_{LE}^{cr} accounting for the linear vdW force only, which is obtained as $F_{LE}^{cr}=-(EI\lambda_1^4+\alpha_1)/\lambda_1^2$ in Sec. II. It is found that this postbuckling load increases with the deflection amplitude and the beam end boundary condition has a significant effect upon this postbuckling equilibrium path, i.e., the change in the postbuckling load causes a larger change in the deflection amplitude for the S-S end condition. To check the beam model effect upon the postbuckling behavior, the deflection amplitude-postbuckling load curve of the embedded CNT with $d=0.7$ nm and $L=10d$ is shown in Fig. 7 for both Euler–Bernoulli and Timoshenko beams with the S-S end condition. The postbuckling loads predicted by these two models are all normalized by the first critical buckling load F_{LE}^{cr} obtained by the Euler–Bernoulli beam theory. The normalized critical buckling load obtained by the linear Timoshenko analysis is 0.995, which is smaller than the Euler–Bernoulli analysis as expected. However, the postbuckling load predicted by the Timoshenko beam is larger than that predicted by the Euler–Bernoulli beam when the deflection amplitude is bigger than a specific value, 0.0095 nm for the current case, for example, which may be also attributed to the fact that the surrounding medium effect is dominant over the effects of the shear deformation and rotary inertia.

In the following analysis, we will focus on the effect of the surrounding medium which exerts a vdW pressure on the CNT surfaces. Figure 8 demonstrates the variation in the resonant frequencies with the length-to-diameter ratio L/d
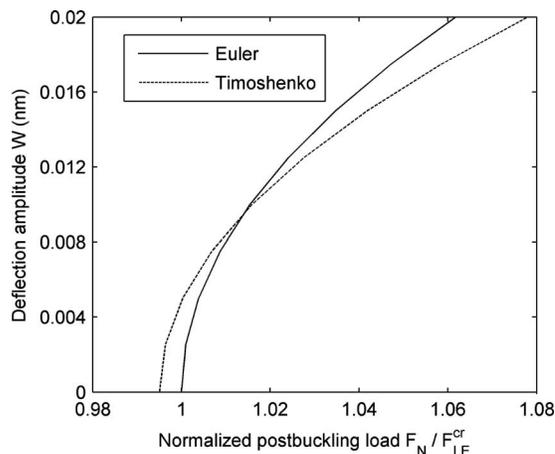
($d=0.7$ nm) for both a free CNT and an embedded CNT using the Euler–Bernoulli beam with the S-S end condition. It is found that the resonant frequencies decrease with the increase in L/d. When L/d is big enough, the resonant frequency of a free CNT (no surrounding medium constrain) approaches to zero as expected. However, the resonant frequencies of an embedded CNT considering the linear vdW force ($\alpha_1 \neq 0$, $\alpha_3=0$) and the nonlinear vdW force ($\alpha_1 \neq 0$, $\alpha_3 \neq 0$, and deflection amplitude $W=0.05$ nm, for example) approach 4.3383 and 5.1962 THz, respectively. The surrounding medium effect upon the applicability and the accuracy of different beam models is also studied by comparing the variation in the critical buckling load ratio F_{LT}^{cr}/F_{LE}^{cr} of a Timoshenko beam to an Euler–Bernoulli beam with the CNT length-to-diameter ratio L/d, as shown in Fig. 9, for the S-S end condition. It is well known that for a free CNT, the Euler–Bernoulli beam model can provide comparable results as the Timoshenko beam model for the beam with large length-to-diameter aspect ratio, for example, $L/d>20$, as shown by the two lower curves in this figure. While considering the surrounding medium effect, the Euler–Bernoulli model may provide accurate results as the Timoshenko model even for the beams with smaller length-to-diameter
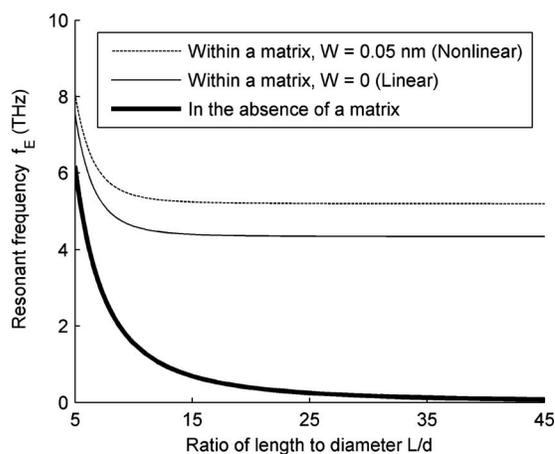
FIG. 8. Variation in the resonant frequencies of an embedded CNT with the L/d ($d=0.7$ nm).
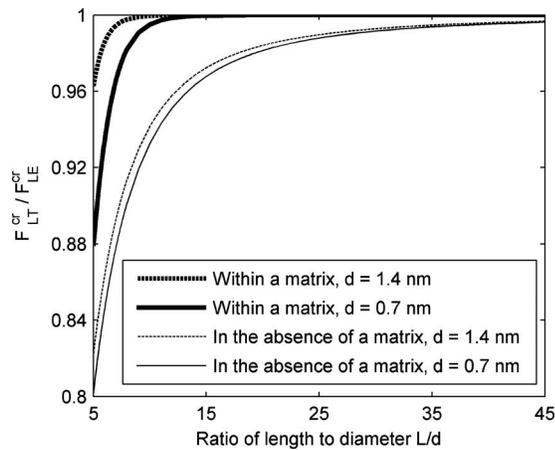
FIG. 9. Variation in the critical buckling load of an embedded CNT with L/d ($d=0.7$ nm).

ratios. This result agrees with the observation by Amin *et al.*[22] when they used the Winkler model to describe the interfacial interaction. It is also observed in this figure that the surrounding medium effect is sensitive to the CNT size. It is concluded from Figs. 8 and 9 that a polymeric matrix has a substantial effect on the vibrational and buckling behaviors of an embedded CNT, which can completely change the expected behavior of a free-standing CNT.

It should be mentioned that the current work aims to study the influence of surrounding medium, i.e., the nonlinear interfacial vdW forces, on the mechanical behavior of embedded CNTs. To address this effect clearly, we studied the nonlinear vibrational and postbuckling behaviors of an embedded single-walled CNT, in which the nonlinearity is caused by the nonlinear vdW forces exerted by the surrounding medium only. However, the methodologies developed in the current work can be extended to study the nonlinear vibration and postbuckling of embedded DWCNTs or MWCNTs, in which the intrinsically nonlinear intertube vdW forces should also be incorporated. The nonlinear vibrational and postbuckling behaviors of DWCNTs or MWCNTs aroused by both the surrounding polymer constraint and intertube interaction are our future concentration.

IV. CONCLUSIONS

In summary, the nonlinear vibration of an embedded single-walled CNT due to the nonlinear vdW interaction forces from its surrounding polymer matrix is studied through Euler–Bernoulli and Timoshenko beam models. The axial load effect and the postbuckling behavior of the embedded CNT are also investigated. The main results of the current work are summarized as follows: (i) Due to the nonlinear interaction forces, the resonant frequencies of the embedded CNT are deflection dependent and the beam end condition has a significant effect upon the deflection amplitude-resonant frequency curves. (ii) Both the CNT diameter and length have a significant effect upon the vibrational behavior of the embedded CNT. (iii) The axial load has a great effect upon the vibrational mode of the embedded CNT. (iv) The nonlinear vdW interaction forces arouse the dependence of the postbuckling load on the deflection ampli-

tude. The postbuckling behavior of the embedded CNT is also significantly affected by the beam end conditions. (v) The applicability and accuracy of Euler–Bernoulli and Timoshenko beam models are affected by the surrounding medium. It is found that the Euler–Bernoulli model may provide comparable results as the Timoshenko beam model even for the CNT beams with small length-to-diameter ratios, for example, $L/d < 10$ or even smaller depending on the CNT size.

[1] S. Iijima, Nature (London) **354**, 56 (1991).
[2] M. M. J. Treacy, T. W. Ebbesen, and J. M. Gibson, Nature (London) **381**, 678 (1996).
[3] B. I. Yakobson, C. J. Brabec, and J. Bernholc, Phys. Rev. Lett. **76**, 2511 (1996).
[4] T. W. Ebbesen, H. J. Lezec, H. Hiura, J. W. Bennett, H. F. Ghaemi, and T. Thio, Nature (London) **382**, 54 (1996).
[5] T. W. Tombler, C. Zhou, L. Alexseyev, J. Kong, H. Dai, L. Liu, C. S. Jayanthi, M. Tang, and S. Y. Wu, Nature (London) **405**, 769 (2000).
[6] M. F. Yu, B. S. Files, S. Arepalli, and R. S. Ruoff, Phys. Rev. Lett. **84**, 5552 (2000).
[7] P. Zhang, Y. Huang, H. Gao, and K. C. Hwang, ASME J. Appl. Mech. **69**, 454 (2002).
[8] P. M. Ajayan and O. Z. Zhou, Top. Appl. Phys. **80**, 391 (2001).
[9] M. S. Dresselhaus and P. Avouris, Top. Appl. Phys. **80**, 1 (2001).
[10] A. Bachtold, P. Hadley, T. Nakanishi, and C. Dekker, Science **294**, 1317 (2001).
[11] J. H. Hafner, C. L. Cheung, and C. M. Lieber, Nature (London) **398**, 761 (1999).
[12] H. J. Dai, Surf. Sci. **500**, 218 (2002).
[13] K. T. Lau and D. Hui, Composites, Part B **33**, 263 (2002).
[14] L. W. Chen, C. L. Cheung, P. D. Ashby, and C. M. Lieber, Nano Lett. **4**, 1725 (2004).
[15] H. R. Lusti and A. A. Gusev, Modell. Simul. Mater. Sci. Eng. **12**, S107 (2004).
[16] Y. Q. Zhang, G. R. Liu, and X. Han, Phys. Lett. A **340**, 258 (2005).
[17] K. Y. Xu, E. C. Mantis, and Y. H. Yan, ASME J. Appl. Mech. **75**, 021013 (2008).
[18] K. Y. Xu, X. N. Guo, and C. Q. Ru, J. Appl. Phys. **99**, 064303 (2006).
[19] Y. M. Fu, J. W. Hong, and X. Q. Wang, J. Sound Vib. **296**, 746 (2006).
[20] J. Yoon, C. Q. Ru, and A. Mioduchowski, Compos. Sci. Technol. **63**, 1533 (2003).
[21] M. Aydogdu, Arch. Appl. Mech. **78**, 711 (2008).
[22] S. S. Amin, H. Dalir, and A. Farshidianfar, Comput. Mech. **43**, 515 (2009).
[23] T. Murmu and S. C. Pradhan, Physica E (Amsterdam) **41**, 1232 (2009).
[24] C. Q. Ru, J. Mech. Phys. Solids **49**, 1265 (2001).
[25] S. Kitipornchai, X. Q. He, and K. M. Liew, J. Appl. Phys. **97**, 114318 (2005).
[26] A. R. Ranjbartoreh, G. X. Wang, A. G. Arani, and A. Loghman, Physica E (Amsterdam) **41**, 202 (2008).
[27] Y. Yan, L. X. Zhang, and W. Q. Wang, J. Appl. Phys. **103**, 113523 (2008).
[28] X. H. Yao and Q. Han, Eur. J. Mech. A/Solids **27**, 796 (2008).
[29] B. I. Yakobson and R. E. Smalley, Am. Sci. **85**, 324 (1997).
[30] L. F. Wang, H. Y. Hu, and W. L. Guo, Acta Mech. Solida Sinica **18**, 123 (2005).
[31] A. Y. T. Leung, X. Guo, X. Q. He, H. Jiang, and Y. Huang, J. Appl. Phys. **99**, 124308 (2006).
[32] D. Qian, E. C. Dickey, R. Andrews, and T. Rantell, Appl. Phys. Lett. **76**, 2868 (2000).
[33] L. S. Schadler, S. C. Giannaris, and P. M. Ajayan, Appl. Phys. Lett. **73**, 3842 (1998).
[34] H. D. Wagner, O. Lourie, Y. Feldman, and R. Tenne, Appl. Phys. Lett. **72**, 188 (1998).
[35] O. Lourie, D. M. Cox, and H. D. Wagner, Phys. Rev. Lett. **81**, 1638 (1998).

[36] R. Parnes and A. Chiskis, J. Mech. Phys. Solids **50**, 855 (2002).

[37] E. T. Thostenson and T. W. Chou, Carbon **42**, 3015 (2004).

[38] C. Li and T. W. Chou, Compos. Sci. Technol. **66**, 2409 (2006).

[39] Y. Lanir and Y. C. B. Fung, J. Compos. Mater. **6**, 387 (1972).

[40] L. Y. Jiang, Y. Huang, H. Jiang, G. Ravichandran, H. Gao, K. C. Hwang, and B. Liu, J. Mech. Phys. Solids **54**, 2436 (2006).

[41] Y. Z. Liu and L. Q. Chen, *Nonlinear Vibration* (High Education, Beijing, 2001) (in Chinese).

[42] G. R. Cowper, ASME J. Appl. Mech. **33**, 335 (1966).

[43] Z. C. Qiao, Appl. Math. Mech. **14**, 517 (1993).

[44] C. L. Amba-Rao, J. Acoust. Soc. Am. **42**, 900 (1967).

[45] S. S. Rao, *Mechanical Vibrations*, 4th ed. (Prentice-Hall, Englewood Cliffs, NJ, 2004).

[46] A. Ramezani, A. Alasty, and J. Akbari, ASME J. Vibr. Acoust. **128**, 611 (2006).